arXiv:cond-mat/0602595v1 [cond-mat.stat-mech] 24 Feb 2006

Cluster growth and dynamic scaling in a two-lane driven diffusive system

I. T. Georgiev[1,2], B. Schmittmann[1] and R. K. P. Zia[1]

[1]Center for Stochastic Processes in Science and Engineering, Department of Physics, Virginia Tech, Blacksburg, VA 24061-0435, USA;
[2]Integrated Finance Limited, 630 Fifth Avenue, Suite 450, New York, NY 10111, USA

Abstract. Using high precision Monte Carlo simulations and a mean-field theory, we explore coarsening phenomena in a simple driven diffusive system. The model is reminiscent of vehicular traffic on a two-lane ring road. At sufficiently high density, the system develops jams (clusters) which coarsen with time. A key parameter is the passing probability, γ. For small values of γ, the growing clusters display dynamic scaling, with a growth exponent of 2/3. For larger values of γ, the growth exponent must be adjusted, suggesting the ordered (jammed) state is not a genuine phase but rather a finite size effect.

E-mail: igeorgiev@iflt.com, schmittm@vt.edu, rkpzia@vt.edu

Submitted to: *J. Phys. A: Math. Gen.*

1. INTRODUCTION

Coarsening phenomena and pattern formation are fascinating subjects, drawing much attention especially in the context of first order transitions [1, 2, 3]. Though these phenomena are inherently dynamic in nature, there are intimate links to the statics associated with thermal equilibrium. To be specific, the underlying rules of evolution of this class of systems obey detailed balance (microscopic reversibility); otherwise, these systems would never reach their equilibrium states. More recently, considerable attention has been directed at a different class of many-body systems, namely, those which settle into *non-equilibrium* steady states. Unlike their equilibrium counterparts, these steady states experience net *fluxes* (of, say, energy or particles) *through* the system. As a result, their stationary distributions lie in general entirely outside the Boltzmann-Gibbs paradigm, and most are completely unknown. Nevertheless, these systems are ubiquitous in nature (including, in particular, *all* biological systems) and deserve our attention. The main distinguishing feature of non-equilibrium steady states is that they are coupled to more than one energy (or particle) reservoir, so that the underlying dynamics *violates* detailed balance. Not surprisingly, such systems display much richer behavior than those in thermal equilibrium [4, 5]. Here, we ask a natural question: If

such a system undergoes a first-order-like transition, will it also display very different coarsening phenomena? In other words, can we expect novel properties in systems evolving under a detailed balance violating dynamics?

Posed in this way, our question is extremely broad and progress towards an answer will not be easy. One approach to this goal is to study idealized, simple model systems. The hope is that, by exploring their behavior, we will gain important insight towards the understanding of more complex real systems. In addition, we may discover universality classes which encompass both simple models and real systems. The Ising model played precisely such a role in the understanding of thermodynamic singularities in an wide class of equilibrium systems. In the same spirit, we explore coarsening phenomena in a simple lattice gas model, driven into steady states far from thermal equilibrium.

Our model is a member of a class known as driven diffusive systems. Introduced by Katz, Lebowitz and Spohn [6] as a seemingly trivial modification of the Ising lattice gas, the prototype displayed many surprising and counterintuitive phenomena. Since then, variations and extensions of this simple model have been explored, and rich and complex behavior continues to emerge [4, 5]. One recent example is the drastic difference between a strictly one dimensional system ($L \times 1$, also refered to as "one-lane") and a quasi-one dimensional ($L \times 2$, "two-lane") lattice gas involving two species of particles [7]. Driven in opposite directions on lattices with periodic boundary conditions ("ring roads"), two particles encountering one another may exchange positions with a small exchange rate γ. The steady state of the *one-lane* model is known analytically [8] to remain homogeneous at all positive γ and $\bar{\rho}$, the *average* particle density or filling fraction. Meanwhile, Monte Carlo studies of the *two-lane* system showed a transition to an *in*homogeneous state, with a single macroscopic cluster [7] (a jammed state). Subsequently, simulations and a mean-field theory for a very similar model also indicated such a kind of "phase transition" [9, 10]. Remarkably, an exact solution for this model was established later [11, 12], showing that the jammed state is a finite-size effect: Two-particle correlations are controlled by a *finite* - but gargantuan (e.g., 10^{70}!) - length scale. Though there are reasons to believe that our model also displays this type of finite-size effect [13, 14, 15], it is nevertheless interesting to investigate jamming, and the growth of jams, in finite systems. In particular, if the crossover to the asymptotic behavior does not occur until the system sizes also reach $O\left(10^{70}\right)$, then it is irrelevant for all conceivable earthbound systems (e.g., pedestrian traffic and biological motors).

With these considerations in mind, we explore coarsening phenomena in the two-lane system, as it evolves toward a jammed state. In a recent study of this model [16, 17], clusters were found to grow much faster than in typical non-driven diffusive systems [1, 2, 3]. Here, we report an in-depth investigation, using both simulation and analytic techniques. Focusing on dynamic scaling of the clustering process, we investigate the average cluster size as a function of time and system size. On the analytic side, we present a set of mean-field equations of motion for the local particle densities. The numerical solutions of these equations resemble the behavior of the exact solution of the deterministic Burgers equation. From the Monte Carlo simulations, in the small γ

regime, we find a growth exponent of 2/3 and good evidence of dynamical scaling. Yet, as γ increases, we are forced to adjust the scaling exponents in order to collapse the data onto a universal curve. We believe that these findings provide further evidence for the destabilization of the ordered "phase" with increasing γ or system size.

2. The model and its properties

The model is defined as a stochastic driven lattice gas with random sequential dynamics that conserves the number of particles. There are two kinds of particles, "positive" (+) and "negative" (−) ones, that perform biased diffusion on an $L \times 2$ lattice with periodic boundary conditions in both directions. Each site on the lattice can be empty ($\oslash$) or occupied by at most one (positive or negative) particle. There are no other interactions between the particles except an excluded volume interaction. The two species are driven in opposite directions by an external field along the x-axis, where $x = 1, ..., L$ labels the position of a site "along the road". The particles can also change lanes (with $y = 1, 2$ being the lane label). One Monte Carlo step (MCS) contains the following steps repeated $2L$ times:

- randomly pick a bond connecting two nearest-neighbor sites on the lattice;
- if the bond is in the x-direction and connects either a ($+\oslash$) or a ($\oslash-$) pair, exchange the particle and the vacancy (a particle-hole exchange). If it is a particle pair ($+-$), then perform the exchange with probability γ - a process also referred to as charge-exchange, or passing in the language of traffic models;
- if the bond is in the transverse direction (cross-lane), then exchange particle-hole pairs always and execute charge exchanges with probability γ.

Since no backward jumps are allowed, these dynamical rules can be interpreted as imposing an infinite external "electric field" on the "charged" particles, which perform random walks *biased* only along x. Apart from the random choosing of bonds, the only stochastic parameter in the model is the particle-exchange probability γ. Our dynamics is invariant under spatial translations and charge-parity (CP) transformations. We have studied only the case of a neutral system, i.e. $N_+ = N_-$, where N_+ and N_- are the number of + and − particles respectively. Further, we focus mostly on systems at half filling, i.e., $0.5 = \bar{\rho} \equiv (N_+ + N_-) / (2L)$.

Unlike its equilibrium analogue, i.e., the Ising model, there is a qualitative difference between the $L \times 2$ (quasi 1-D) and the $L \times 1$ (strictly 1-D) systems. For the latter case, both the exact solution (for an infinite system) [8] and computer simulations (of finite systems) [18] show that the steady state is disordered and homogeneous. Specifically, if we define a cluster as a collection of particles connected by nearest-neighbor bonds, then the distribution of cluster sizes is controlled by an exponential with a characteristic length of $O(L^0)$, remaining finite except in the singular limits $\gamma \to 0$ or $\bar{\rho} \to 1$. By contrast, the presence of a second lane has a profound effect on the steady state. For large regions in the γ-$\bar{\rho}$ plane, the cluster-size distribution



Figure 1. Space-time plot of a 512×2 lattice with particle density $\bar{\rho} = 0.5$ and charge-exchange probability $\gamma = 0.2$. The initial configuration is random. For each x, a black dot represents particles in both lanes, a white dot represents no particles, and a gray dot represents one of the two lanes being occupied.

has another peak located at sizes $\propto L$, which is a clear signal of a macroscopic jam [7, 16, 17, 15]. This behavior is very counterintuitive: Adding a second lane should not lead to worse traffic jams! According to one's naïve expectation, the extra degree of freedom associated with the additional lane should provide an efficient mechanism for relieving blockages and allowing the system to reach a more homogeneous state. Instead, computer simulations reveal properties more akin to the 2-D system ($L \times L$), where a compact, macroscopic cluster is present in significant portions of the γ-$\bar{\rho}$ phase diagram. Although the macroscopic cluster in the $L \times 2$ case is unlikely to persist in the $L \to \infty$ limit [15], our focus here is how the system evolves toward a phase-separated state in (physically reasonable) L's up to $O(10^5)$.

Just like in the daily commute, for low γ and moderate $\bar{\rho}$, a local blockage will remain long enough for the next group of particles to jam into it. As a result, the blockage grows, as long as the influx, due to the arrival of particles from *outside* the cluster, exceeds the outflux, due to the loss of particles from non-zero γ. Fig. 1 provides an example of this growth process. It is a space-time plot of a 512×2 lattice starting from a random initial configuration. The overall particle density is $\bar{\rho} = 0.5$ (i.e. $\bar{\rho}_+ = \bar{\rho}_- = 0.25$) and the charge-exchange probability is $\gamma = 0.2$. Each row on the figure encodes the microscopic configuration on the lattice. Time runs vertically downwards, covering the first 400 MCS. For these values of L, $\bar{\rho}$, and γ, the system will coarsen until there is only one macroscopic cluster. The remainder of this paper will be devoted to a more quantitative characterization of this coarsening process. Before continuing, let us provide some necessary definitions.

First, we define a cluster of size s as any s particles connected by nearest-neighbor bonds regardless of their charge (i.e., a "mass" cluster). By collecting a histogram of

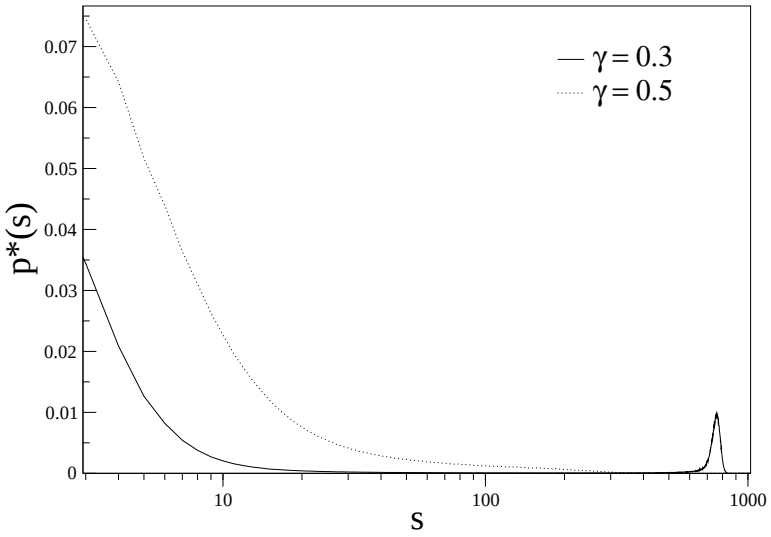


Figure 2. The residence distribution for two values of γ on a 1024×2 lattice, for $\bar{\rho} = 0.5$. For $\gamma = 0.3$ we observe the ordered phase with a bi-modal distribution (a decay for small values of s and a peak corresponding to the macroscopic cluster), while for $\gamma = 0.5$ we have a disordered phase with uni-modal residence distribution.

cluster sizes formed at time t, we can estimate the probability $\tilde{p}(s,t)$ of having a cluster with a mass s at time t. Since $\tilde{p}$ is not a conserved distribution, it is customary to study the residence distribution, defined as $p(s,t) \equiv s\ \tilde{p}(s,t)$. Representing the probability that a randomly chosen particle belongs to a cluster of size s at time t, this distribution is easily normalized, i.e., $\sum_s p(s,t) = 1$. The steady-state residence distribution $p^*(s)$ is given by $p^*(s) = \lim_{t\to\infty} p(s,t)$. In the 1-lane system, it is monotonically decreasing and, in the thermodynamic limit, known analytically : $p^*(s) \propto s^{-1/2} \exp(-s/\xi)$ [8], where $\xi(\bar{\rho},\gamma)$ is a characteristic mass independent of L. However, for the 2-lane model, p^* changes from being monotonic for larger values of γ to being bi-modal for small γ (and moderate $\bar{\rho}, L$). An example is shown in Fig. 2, where $\bar{\rho} = 0.5$, $L = 1024$, and γ takes two values, 0.5 and 0.3. For the larger γ, p^* is similar to the 1-lane case. For the smaller value, p^* has a second peak at $s = O(L)$, associated with the macroscopic cluster. Meanwhile, the peak at $s = 0$ can be traced to the region *outside* this cluster, where a very low particle density allows only for very small blockages ($s \leq 5$). We refer to the particles in this region as "travellers" (see also Fig. 1). Further details about the stationary states and the γ-$\bar{\rho}$ phase diagram can be found in [15].

3. Monte Carlo simulations

In a preliminary study of coarsening in this model [16, 17], systems up to $L = 10^4$ with $\gamma = 0.1$ were simulated. The main observation is that the cluster sizes appear to grow roughly as $t^{2/3}$. Here, we report the results of a refined study using a fast multi-spin

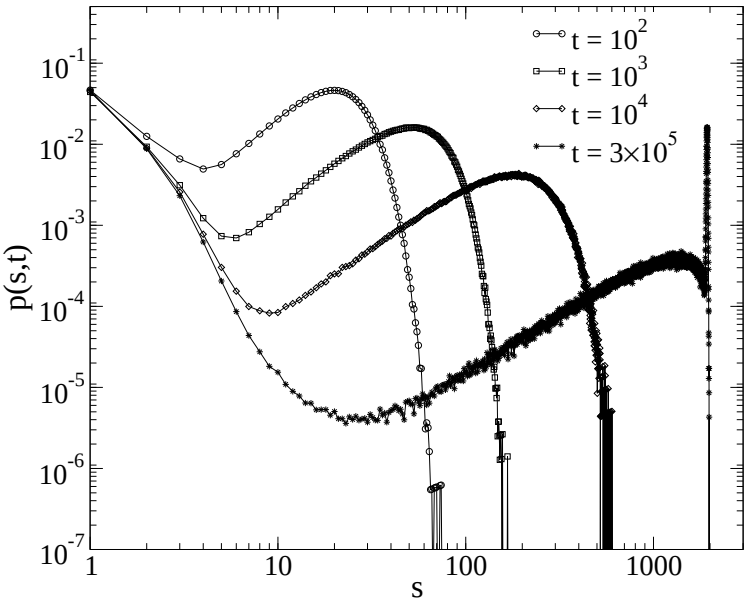


Figure 3. The residence distribution $p(s,t)$ *vs* the cluster mass s at different times $t = 10^2, 10^3, 10^4$ and 3×10^5 MCS. The lattice size is $L = 2048$ with $\gamma = 0.1$ and $\bar{\rho} = 0.5$.

coding algorithm where the storage of the microstates on the lattice and the updating rules are coded in a bit-wise manner, as in, say, [19]. Since our model is a three-state model, we need at least two bits to store the three possible states on a single lattice site. Instead of using two consecutive bits in a machine word for encoding the state on a site, we prefer to use one bit from two different words. In this way the algorithm for a single Monte Carlo step becomes somewhat simpler, though working with two different arrays representing the two lanes reduces the efficiency slightly. Each element of the two arrays represents a particular site on one of the lanes. Exploiting the 64-bit architecture of our hardware, the individual bits in the machine word encode the state on this site for 64 different lattices, all of which are updated simultaneously. The increase in the efficiency of the multi-spin algorithm is roughly 35-fold over the standard single spin flip algorithm. This allows us to study much larger systems and provides much better statistics.

Fig. 3 shows the behavior of the residence distribution $p(s,t)$ on a 2048×2 lattice with $\gamma = 0.1$ and particle density $\bar{\rho} = 0.5$. In the regime from $\sim 10^2$ to $\sim 10^5$ MCS, seemingly unbounded coarsening occurs. Thereafter, the largest cluster saturates the system size and the system settles into a steady state. Two components of $p(s,t)$ are easily distinguished, corresponding to a relatively static mode near the origin associated with the travelers, and a more "dynamic" mode associated with the growing clusters. Since these modes exhibit drastically different time dependences, the full distribution cannot be collapsed on a single universal curve. We can, however, isolate the "growing" component by introducing a coarse-grained description of the growth process [16].

We define a strictly one-dimensional coarse-grained configuration on a $L \times 1$ chain

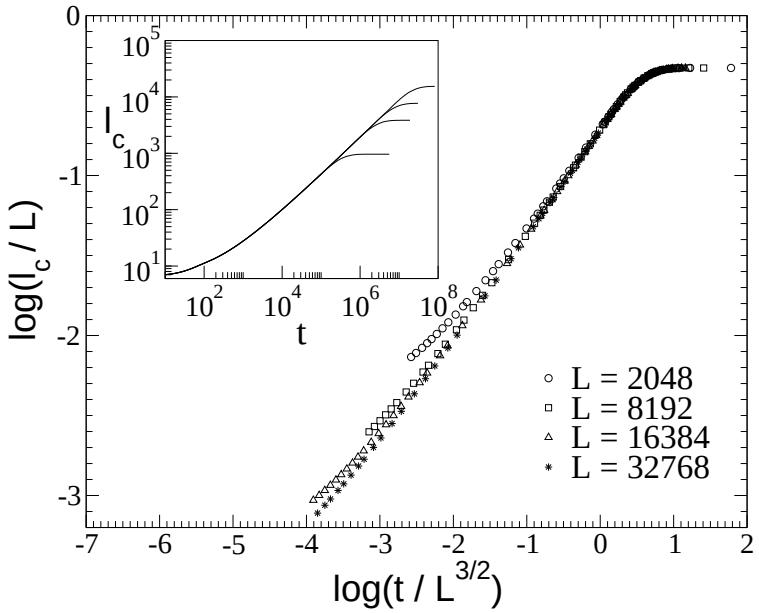


Figure 4. Dynamic scaling for l_c/L^α vs. t/L^z for $\gamma = 0.1$ and $\bar{\rho} = 0.5$. The graphs collapse on an universal curve for large t with $\alpha = 1.0$ and $z = 3/2$. The inset shows the original data l_c vs. t, where the lattice sizes are $L = 2048, 8192, 16384$ and 32768 from top to bottom.

as follows: (i) for a suitably chosen positive integer b, center a $b \times 2$ window at each site $x = 1, ..., L$ with, say, $y = 1$ of the original lattice and count the number of particles inside the window; (ii) if this particle number exceeds b, we occupy the associated site x on the (coarse-grained) $L \times 1$ lattice; otherwise, that site remains empty. Clearly, this procedure is independent of y, i.e., which lane is selected. Since the small clusters in the traveler region rarely exceed a mass of 5, we use windows of length $b = 5$. As a result, the traveler component is removed from the coarse-grained configuration which contains only the information about the growth mode. Since large clusters are almost unaffected by the coarse-graining procedure, it should be obvious that the large-scale dynamics on the new $L \times 1$ lattice has the same characteristics as the original system. The coarse-graining procedure is performed each time we take data, and the information about the lengths of clusters on the new lattice is collected. The coarse-grained residence distribution, $p(l, t)$, on the new lattice is defined as before, namely, as the (normalized) probability that a randomly chosen particle belongs to a cluster of length l at time t. The average cluster length $l_c(t)$ is defined as its first moment:

$$l_c(t) \equiv \sum_{l=1}^{L} l \; p(l, t) \tag{1}$$

In the following, we show two large data sets for l_c vs. t obtained from 4096 independent runs, on lattices with $L = 2K$, $8K$, $16K$, and $32K$, and $\bar{\rho} = 0.5$. One data set shows a relatively small value of γ, $\gamma = 0.1$ (Figs. 4 and 5); the other shows the significantly larger value $\gamma = 0.3$ (Figs. 6 and 7). All initial ($t = 0$) configurations are random.

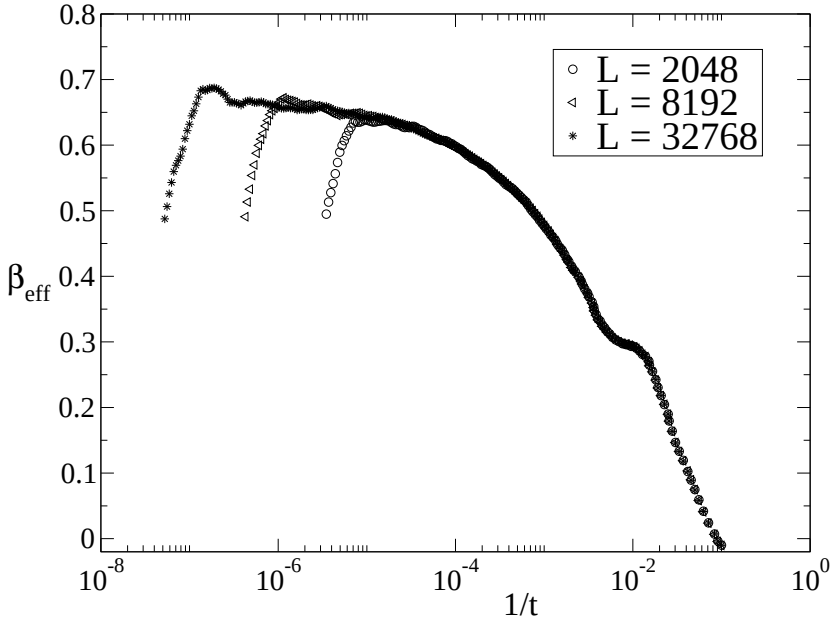


Figure 5. The effective growth exponent β_{eff} for $\gamma = 0.1$ and lattice sizes $L = 2048, 8192$ and 32768.

To analyze the data, we test whether they satisfy dynamic scaling of the form:

$$l_c(t) = L^{\alpha}\, F(t/L^z) \tag{2}$$

This scaling form is chosen to reflect two features of our data. On the one hand, on any given lattice, we expect a saturation of cluster sizes for large times, so that $\lim_{t\to\infty} l_c(t)$ should become independent of time. In other words, the scaling function $F(x)$ should approach a constant as $x \to \infty$. Any L-dependence of the steady-state cluster size is reflected in the exponent α, via $\lim_{t\to\infty} l_c(t) \propto L^{\alpha}$. On the other hand, we check whether the growth regime follows a power law, corresponding to $l_c(t) \propto t^{\alpha/z}$ and a finite limit of $x^{-\alpha/z}F(x)$ for $x \ll 1$. For $\gamma = 0.1$, the data collapse is very good at large t, using the exponent values $\alpha = 1.00 \pm 0.01$ and $z = 1.50 \pm 0.01$. This gives us a cluster growth exponent $\beta \equiv \alpha/z = 0.66 \pm 0.02$ consistent with a value of 2/3. It is not surprising, of course, that the scaling form of Eq. (2) does not hold for early times. Starting from random configurations, particles immediately follow their preferred direction, rapidly generating many small clusters separated by completely empty regions. The associated $l_c(t)$ is nearly constant for some time and independent of system size, so that the corrections to Eq. (2) decrease with L. The average cluster size only starts to increase noticeably when particles begin to escape from these small clusters, initiating the growth regime.

To put the spot light squarely on the growth regime, we show the local exponent, $\beta_{eff} \equiv d\ln(l_c(t))/d(\ln t)$ in Fig. 5, for a range of system sizes. This representation is of course much more sensitive to small changes in the power law, $l_c(t) \propto t^{\beta_{eff}}$, than Fig. 4. The data show that β_{eff} is monotonically increasing with t and independent of L until the saturation regime sets in. The onset of saturation is marked by a sharp spike

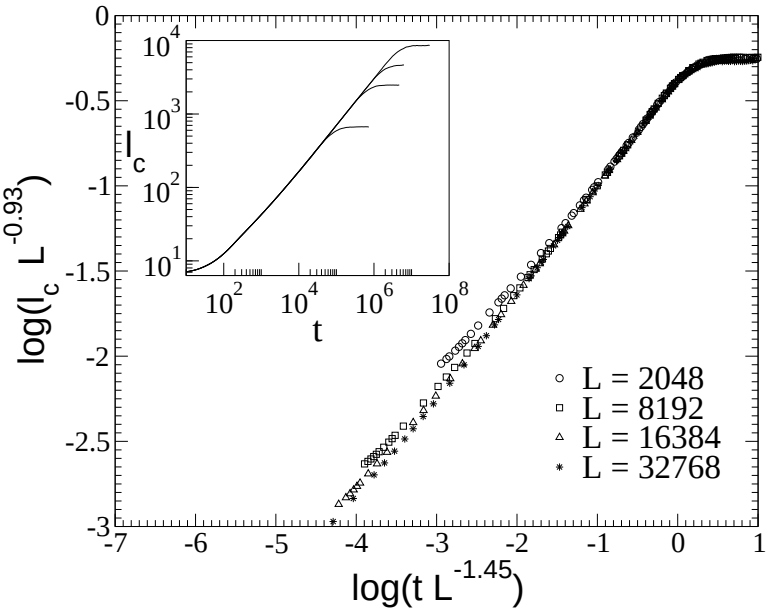


Figure 6. Dynamic scaling for l_c/L^α vs. t/L^z for $\gamma = 0.3$ and $\bar{\rho} = 0.5$. The graphs collapse on an universal curve for large t with $\alpha = 0.93$ and $z = 1.45$. The inset shows the original data l_c vs. t, where the lattice sizes are $L = 2048, 8192, 16384$ and 32768 from top to bottom.

in β_{eff}, followed by a similarly sharp drop. Just before saturation, β_{eff} approaches the limiting value 2/3. The apparent t-dependence of β_{eff} simply reflects the behavior of the scaling function $F(t/L^z)$. The behavior of our system after saturation, reflected in the exponent value $\alpha = 1.0$ shows that the largest clusters are indeed macroscopic, in that their size scales linearly with L.

The results for the case of $\gamma = 0.3$ are shown in Figs. 6 and 7. By increasing γ, we effectively destabilize the macroscopic clusters in the stationary regime. Here, the best data collapse is obtained with $\alpha = 0.93 \pm 0.01$ and $z = 1.45 \pm 0.01$, which results in a growth exponent $\beta = 0.64 \pm 0.02$. The smaller value of β is also clearly reflected in the plot of the local slope, Fig. 7. The need to adjust the scaling exponents as functions of γ may well point towards significant changes in the steady-state properties of the model. For sufficiently large L and γ, a crossover to an exponential (rather than bi-modal) residence distribution occurs [15]. For our parameters ($\bar{\rho} = 0.5$, $\gamma = 0.3$, $L \leq 32k$), the stationary distribution is still bi-modal but the peak at large s is already very broad. While the data collapse for the coarsening system is still very good, a value of $\alpha < 1$ shows that the largest clusters already scale sublinearly with L. It is conceivable that Eq. (2) acquires additional corrections which account for the crossover, leading to effectively γ-dependent exponents. For $\gamma = 0.37$ (Fig. 8) it becomes blatantly obvious that β_{eff} remains well below 0.6 and that there are strong L-dependent corrections.

To summarize, for small values of γ (i.e. $\gamma \leq 0.1$), the system coarsens with a growth exponent β consistent with 2/3, and approaches a steady state characterized by a single macroscopic cluster, with $l_c \propto L$. As γ increases, the data collapse remains

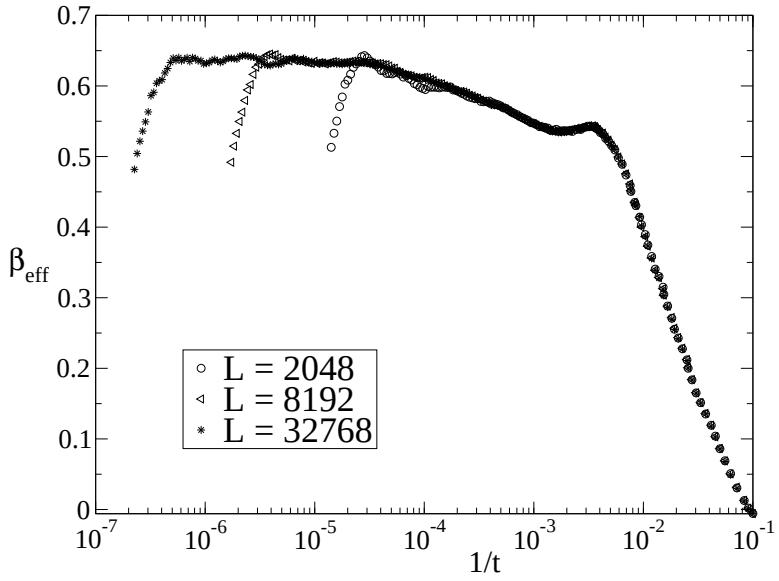


Figure 7. The effective growth exponent β_{eff} for $\gamma = 0.1$ and lattice sizes $L = 2048, 8192$ and 32768.

good but only if the exponents are adjusted with γ. In particular, the growth exponent β must be reduced quite significantly. It is natural to conclude that this is a by-product of the crossover from bi-modal to exponential $p^*(s)$.

4. A mean-field approximation

Noise plays a significant role in our Monte Carlo simulations. First, all initial conditions are random; second, and more importantly, the dynamics itself is inherently stochastic. Even starting from the same initial condition, each Monte Carlo run follows a distinct trajectory. It is natural to ask whether the statistical averaging over these different trajectories is essential for the coarsening process. To put this question into context, we recall that thermal fluctuations play no role for the temporal evolution of equilibrium systems towards their final ordered states, provided the domain size is much larger than the thermal correlation length [3]. As a result, domain growth laws can be obtained by integrating a deterministic mean-field equation, e.g., the Cahn-Hilliard equation for the ordering dynamics of a scalar conserved order parameter (Model B, in the Hohenberg-Halperin classification [20]).

In this section, we neglect fluctuations, in an attempt to test their relevance. We establish evolution equations for the two particle densities which form the analogue of the Cahn-Hilliard equation for our dynamics and integrate them numerically. The only source of noise will be in the initial condition; once it is set, the evolution proceeds completely deterministically. If we recover a growth exponent of 2/3, we may conclude that the stochasticity of the Monte Carlo simulations is irrelevant. In contrast, if a different growth exponent emerges here, we are faced with a stark difference between coarsening towards an equilibrium vs a non-equilibrium steady state, namely, that

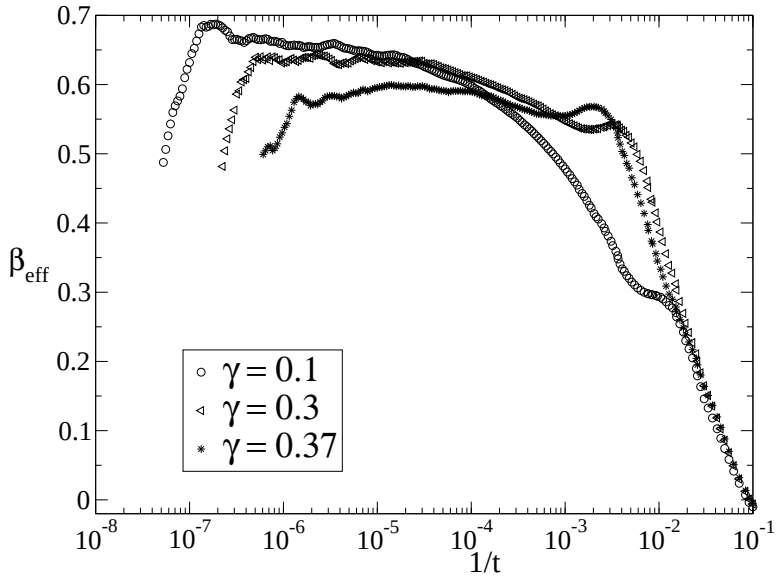


Figure 8. The effective growth exponent β_{eff} for $\gamma = 0.1, 0.3$ and 0.37 for lattice size $L = 32768$.

fluctuations are essential to describe coarsening phenomena in the latter.

To obtain a set of evolution equations, we begin from the microscopic master equation and derive equations for the local averages, $\langle \rho^+(x,y,t) \rangle$ and $\langle \rho^-(x,y,t) \rangle$, of positive and negative particles at lattice site x, y and time t. Alternatively, we can write down simple balance equations for the loss and/or gain of particles at a given lattice site. Since the numerical integration will require a discrete spatial variable, we simply work with the original lattice, rather than taking a naive continuum limit. We assume spatial homogeneity in the y-direction, letting the densities depend on x only, $\langle \rho^+(x,y,t) \rangle \to \langle \rho^+(x,t) \rangle$. In a mean-field approximation, all higher-point averages are replaced by products of one-point averages, e.g., $\langle \rho^+(x+1,t)\rho^-(x,t) \rangle \simeq \langle \rho^+(x+1,t) \rangle \, \langle \rho^-(x,t) \rangle$. Finally, for simplicity, we omit the $\langle \cdot \rangle$ brackets, and introduce the local hole density:

$$\phi(x,t) \equiv 1 - \rho^+(x,t) - \rho^-(x,t)$$

The resulting equations, in one spatial dimension, are given by [21]:

$$\begin{aligned} \partial_t \rho^+(x,t) &= \rho^+(x-1,t)\phi(x,t) - \rho^+(x,t)\phi(x+1,t) \\ &\quad + \gamma \left[\rho^+(x-1,t)\rho^-(x,t) - \rho^+(x,t)\rho^-(x+1,t) \right] \\ \partial_t \rho^-(x,t) &= \rho^-(x+1,t)\phi(x,t) - \rho^-(x,t)\phi(x-1,t) \\ &\quad + \gamma \left[\rho^-(x+1,t)\rho^+(x,t) - \rho^-(x,t)\rho^+(x-1,t) \right] \end{aligned} \tag{3}$$

Each of the terms on the right hand side is easily understood; for example, the contribution $\rho^+(x-1,t)\phi(x,t)$ reflects the jumps of positive particles at site $x-1$ to site x, provided x is empty. The equations for $\rho^+(x,t)$ and $\rho^-(x,t)$ are of course related by a charge-parity (CP) symmetry. The two equations take the form of continuity equations, i.e.,

$$\partial_t \rho^\pm(x,t) = j^\pm(x-1,t) - j^\pm(x,t) \tag{4}$$

where $j^+(x,t) \equiv \rho^+(x,t)\,[\phi(x+1,t)+\gamma\rho^-(x+1,t)]$ and $j^-(x,t) \equiv -\rho^-(x+1,t)\,[\phi(x,t)+\gamma\rho^+(x,t)]$ denote the net currents of positive and negative particles from site x to site $x+1$, respectively.

Before we turn to the numerical integration of these equations, we first summarize the key properties of their *stationary* solutions, $\rho^+(x,t) \to \rho^+(x)$ and $\rho^-(x,t) \to \rho^-(x)$. This will help us interpret the density profiles at late times. Since Eqns. (3) take the form of continuity equations, they are clearly satisfied by spatially uniform densities, reflecting homogeneous steady states. In the *continuum* limit, spatially inhomogeneous stationary solutions, reflecting jammed states, can also be found [21]. These consist of a domain of travellers (characterized by uniform densities) and a single large cluster, containing essentially no holes (i.e., $\phi \simeq 0$ inside), linked by a narrow region in which the densities vary rapidly, reminiscent of shocks. Remarkably, it is straightforward to find *approximate* solutions to Eqns. (3) which consist of separate uniform and cluster domains, patched together by a consistency condition. Stationarity implies $j^\pm(x,t) \equiv j^\pm = const$ independent of t and x. The CP symmetry also leads to $j^+ = -j^- \equiv j$. In the traveller domain, all densities are uniform whence $j = \rho^+\,[\phi+\gamma\rho^-]$. Invoking symmetry again, we expect $\rho^+ = \rho^- \equiv \rho$, and $\phi = 1-2\rho$ so that we can find the current-density relation in the traveller domain:

$$j = \rho\,[1-2\rho+\gamma\rho] \tag{5}$$

Next, we center the x-axis in the middle of the cluster and simplify Eqns (3) by setting $\phi(x) = 0$, i.e., $1 = \rho^+(x) + \rho^-(x)$. By continuity, the currents inside the cluster must equal the exterior currents whence

$$j = \gamma\rho^+(x)\rho^-(x+1) = \gamma\rho^+(x)\left[1-\rho^+(x+1)\right] \tag{6}$$

This is a recursion relation for $\rho^+(x)$, solved by

$$\rho^+(x) = \frac{1}{2}\,[1 - A\tan\mu x] \tag{7}$$

with the amplitude and slope of the tan-function given in terms of the excess current, $j_{ex} \equiv j - \gamma/4 > 0$, via

$$A = \tan\mu = \sqrt{j_{ex}}$$

Clearly, the corresponding negative charge density is given by $\rho^-(x) = 1-\rho^+(x)$. To match the solutions inside and outside the clusters, we note that the positive particles form a sharp shock front at the *left* edge of the cluster while behaving quite smoothly at the *right* edge [22]. Assuming the cluster ranges from $x = -l/2$ to $x = +l/2$, we match the interior density to the exterior one by equating them at the *right* edge:

$$\rho = \rho^+(l/2)$$

To close the set of equations, one must add the overall mass constraint, $2\bar{\rho}L = l + 2\rho(L-l)$ to these relations.

The two key results from this section are (i) the tan-shape of the density profiles inside a stationary cluster, and (ii) the excess current j_{ex} through a cluster of length

l. Instead of the lengthy full expression, we only give its form for large l, namely, $j_{ex} \simeq \pi^2\gamma/l^2$.

To solve the mean-field equations numerically, we use a simple Euler integration scheme, which is stable for our set of equations. The maximum number of space discretization points that we have used is 10^5 and the time propagation is achieved by using a step $\delta t = 0.4$. The initial values for the densities are digitized, i.e. they take only the values 0.0 and 1.0 at the different space locations according to the chosen particle density. As in the Monte Carlo simulations, we restrict ourselves to a particle density of 0.5, and choose $\gamma = 0.1$. To define a cluster, we set a threshold value $\phi_{th} = 0.3$ for the density of the holes, i.e. the point x where $\phi(x)$ crosses ϕ_{th} from above (below) marks the beginning (end) of a cluster. To compute the average cluster size $\bar{l}_c(t)$, we average over 4000 independent random initial configurations, using the same method as in the Monte Carlo simulations.

Following the evolution of a typical initial condition, we can distinguish several stages. Within the first few time steps, the sharp distinction between initially filled ($\phi(x,0) = 0$) and initially empty ($\phi(x,0) = 1$) regions blurs. Domains of positive density ($\rho^+(x,0) = 1$) leak rapidly to higher x-values until they encounter domains of negative density. At $t \sim 100$, larger domains of high mass density have formed, typically covering $15-20$ discretization points. Even though the mass density in these clusters is not always fully saturated, almost all of these regions are included in the cluster count, due to the fairly high threshold value, $\phi_{th} = 0.3$. Considering the two particle densities, we observe that the left (right) edges of clusters are marked by sharp peaks in ρ^+ (ρ^-). Highly saturated domains are characterized by two peaks which are almost perfect mirror images of one another. The traveler regions are still quite inhomogeneous and evolve rapidly. At later times (e.g., $t \sim 1000$), these traveler regions have become much more uniform, and essentially all clusters have a mass density near unity. Moreover, it appears that the density profiles inside the clusters develop a tan-shape reminiscent of the stationary solution, Eq. (7). In other words, the late-time profiles can be described as being patched together from alternating traveller and cluster domains, each of which seems nearly "equilibrated" within itself but not yet in "equilibrium" with the others. We will return to these observations below.

Our results for the average cluster size, $\bar{l}_c(t)$, and for the local growth exponent $\bar{\beta}_{eff} \equiv d\ln(\bar{l}_c(t))/d(\ln t)$ are shown in Fig. 9. At early times ($t \sim 100$), the local growth exponent develops a pronounced peak which can be traced to the rapid formation of partially unsaturated clusters. Not surprisingly, the detailed behavior of $\bar{\beta}_{eff}$ in this regime is very sensitive to the chosen threshold ϕ_{th}. A lower ϕ_{th} will reduce the size of this peak. For later times, the mean-field $\bar{\beta}_{eff}$ behaves very similarly to its Monte Carlo counterpart. It slowly approaches a limiting value 0.63 ± 0.01 before the system reaches steady state. As in the MC simulations, the limiting value "creeps up" as the number of space discretization points (the system size) increases, so that the mean-field results appear to be are consistent with a growth exponent of 2/3.

Let us conclude this section by discussing a few simple analytic attempts towards

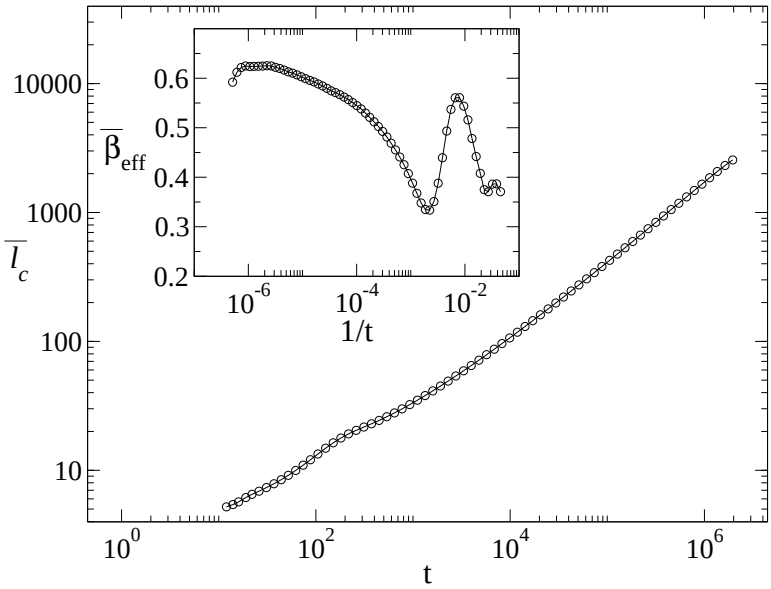


Figure 9. The average cluster size $\bar{l}_c(t)$ and the effective growth exponent β_{eff} for $\gamma = 0.1$ from mean-field numerical simulations.

computing the growth exponent. None of them generate a satisfactory estimate of the growth exponent, whence we conclude that its origin may be quite subtle. Taking our clues from the Monte Carlo simulations, we note that particles spend only a negligeable amount of time in transit between clusters. Moreover, the density of travellers remains approximately constant in time. It seems therefore reasonable to focus on the sizes (lengths) of the clusters only. These evolve as neighboring clusters exchange particles. Starting from the strictly one-dimensional coarse-grained configurations described in Section (3), the simplest representation of a sequence ($i = 1, 2, ...$) of clusters is to specify their lengths, l_i, and the net positive and negative particle currents, $j^{\pm}(l_i)$, which flow through them. Assuming that cluster i gains positive (negative) particles from its left (right) neighbor and loses them to its right (left) neighbor, we may write

$$\dot{l}_i = j^+(l_{i-1}) + j^-(l_{i+1}) - \left[j^+(l_i) + j^-(l_i)\right]$$

Clearly, an overall constant cancels on the right hand side, so that only the l-dependent *excess* currents contribute. If we assume that the cluster interiors are nearly "equilibrated" in the latest stages of the growth process and invoke the mean-field result $j^+_{ex}(l_i) \simeq j^-_{ex}(l_i) \propto 1/l_i^2$, simple scaling gives us $\dot{l} \propto 1/l^2$ or $l \sim t^{1/3}$. This clearly produces a poor estimate (1/3) for the growth exponent. A somewhat better – but still unsatisfactory – estimate can be obtained if we replace the mean-field expression for the currents by its exact counterpart. To do so, we recall that the cluster interiors are almost entirely free of holes so that the dynamics inside the clusters is dominated by $+/-$ exchanges, following a totally asymmetric simple exclusion process (TASEP) [23]. The associated excess currents are exactly known: $j^+(l_i) = j^-(l_i) \propto 1/l_i$. Simple scaling now yields $l \sim t^{1/2}$ which is faster than the mean-field estimate but still slower than the observed $t^{2/3}$ behavior. We note briefly that the same exponent ($\beta = 1/2$)

results from a representation of the cluster growth process in terms of coalescing but otherwise noninteracting random walkers [16, 24]. We believe that the deficiencies of these approaches can be traced, by monitoring the evolution of our clusters, to the rapid and systematic disintegration of small ones. While this bias towards larger clusters can be modelled in an ad hoc (but quantitatively very accurate) fashion by introducing appropriate interactions between the walkers [16], we have as yet no reliable insight into the physical origin of these interactions.

Finally, let us offer an intuitive picture which may provide some hints towards a growth exponent of 2/3. First, the strongest evidence for this value results from simulations with small γ. This suggests a time scale separation between the dynamics of the traveller domains, dominated by fast particle-hole exchanges, and the cluster regions, controlled by charge exchanges on a much slower time scale set by γ^{-1}. This is clearly reflected in the mean-field currents, Eqs. (5) and (6). In other words, particles spend only very brief periods travelling from one cluster to the next, compared to the time required to traverse a large cluster from one end to the other. Moreover, the microscopic dynamics within the interior of clusters is a simple TASEP which can be described, under very well-defined conditions [25], by the deterministic Burgers equation [26]. It is therefore tempting to neglect the traveller regions and to think of the sequence of clusters in terms of coarsening Burgers shocks. In this context, it is well known [26] that the average distance of shocks grows as $t^{2/3}$, provided an average over random initial conditions is taken. Of course, this reasoning remains a conjecture until a more rigorous analytic formulation can be found.

5. Conclusions

To summarize, we have analyzed a coarsening phenomenon in a two-species driven diffusive system on an $L \times 2$ periodic lattice. Positive (negative) particles hop in the positive (negative) x-direction with rate 1, provided the destination site is empty. If it is filled by a particle of opposite charge, the exchange occurs with rate $\gamma < 1$. Cross-lane exchanges are unbiased. Since $\gamma < 1$, two opposing particles impede each other, resulting in a temporary local blockage. For sufficiently small γ, or sufficiently high overall particle density, these local jams aggregate ("coarsen") into a macroscopic cluster which characterizes the final steady state of finite systems. A simple interpretation of this dynamics is traffic of fast and slow cars on a two-lane ring road, viewed from a co-moving frame.

Using Monte Carlo simulations and the numerical integration of a set of mean-field equations, we study how an initially random distribution of particles evolves to this inhomogeneous steady state, i.e., we quantify the coarsening process in which local blockages form larger and larger clusters. Measuring the average cluster size, $l_c(t)$, as a function of time, both methods indicate power law growth $l_c(t) \sim t^{\beta}$ with a growth exponent $\beta \simeq 2/3$ for the late stages of growth. In fact, Monte Carlo simulations show excellent data collapse for small γ and a range of system sizes if $l_c(t)/L$ is plotted

vs $t/L^{3/2}$. However, as γ increases, the scaling exponents have to be adjusted to achieve a comparable quality of data collapse. We interpret this as further evidence for the observation that the inhomogeneous stationary state will not survive in the thermodynamic limit [13, 14, 15].

Since the stationary properties of the $L \times 1$ system can be rigorously mapped [13, 14] into an exactly solvable one-dimensional zero-range process (ZRP) [27] involving one species of particles, it is natural to compare our findings to recent results for the coarsening dynamics of such models [28]. They are defined on a chain of sites, each of which can be occupied by an integer number, $k = 0, 1, 2, ...$ of particles. The hopping rate $w(k)$ of a given particle depends only on the number, k, of particles located at the originating site. Under well-defined conditions on the $w\,(k)$, the density in the bulk is limited to a critical value, and excess particles accumulate ("condense") at a non-extensive fraction of sites [27]. Cluster sites are then defined as those sites where a macroscopic fraction of particles has accumulated [28]. As the system approaches the final stationary state, one monitors how the average number of particles at these cluster sites grows with time. Two basic universality classes can be distinguished: If the $w(k)$ are symmetric, i.e., particles hop to the right and left with equal rates, the dynamic exponent is found to be $z = 3$, resulting in a growth exponent $\beta = 1/3$. In contrast, if the particle hopping is biased, the growth occurs faster, with $z = 2$ and $\beta = 1/2$. Clearly, both of these are incompatible with our results. We note that growth exponents of $\beta = 2/3$ can be "engineered" in one-dimensional ZRPs involving *two* species of particles [29], but only for very special rates which break a fundamental symmetry of our dynamics, mainly, CP invariance. Hence, we believe that there is little to learn from these results for our case. Clearly, the fast coarsening observed here, compared to growth exponents of 1/3 or 1/2 indicates that some essential characteristics of our dynamics cannot be captured in the simple ZRP picture. At this point, we can only speculate what these features might be.

Acknowledgments. We thank G. Korniss, J. Krug, M. Evans, Y. Kafri, D. Mukamel, and G. Schütz for helpful discussions. This work is partially supported by the NSF through DMR 0414122.

[1] J.D. Gunton, M. San Miguel, and P. Sahni, in *Phase Transitions and Critical Phenomena*, Vol. 8, eds. C. Domb and J.L. Lebowitz (Academic Press, New York 1983)
[2] J.S. Langer, in *Solids far from Equilibrium*, ed. C. Godrèche (Cambridge University Press, 1992)
[3] A.J. Bray, Adv. Phys. **43**, 357 (1994)
[4] B. Schmittmann and R.K.P. Zia, Statistical mechanics of driven diffusive systems. In: *Phase Transitions and Critical Phenomena*, Vol. 17, eds. C. Domb and J.L. Lebowitz (Academic Press, New York 1995).
[5] D. Mukamel, In: *Soft and Fragile Matter: Nonequilibrium Dynamics, Metastability and Flow*, eds. M.E. Cates and M.R. Evans (IOP Publishing, Bristol, 2000).
[6] S. Katz, J.L. Lebowitz and H. Spohn, Phys. Rev. B **28**, 1655 (1983) and J. Stat. Phys. {34}, 497 (1984)
[7] G. Korniss, B. Schmittmann and R. K. P. Zia, *Europhys. Lett.* **45** 431 (1999).
[8] S. Sandow and C. Godrèche, unpublished (1998).

[9] P. F. Arndt, T. Heinzel and V. Rittenberg, *J. Phys. A: Math. Gen.* **31** L45 (1998).
[10] P. F. Arndt, T. Heinzel and V. Rittenberg, *J. Stat. Phys* **97** 1 (1999).
[11] N. Rajewsky, T. Sasamoto and E. R. Speer, *Physica A* **279** 123 (2000).
[12] T. Sasamoto and D. Zagier, *J. Phys. A: Math. Gen.* **34** 5033 (2001).
[13] Y. Kafri, E. Levine, D. Mukamel, G. M. Schütz and J. Török, *Phys. Rev. Lett.* **89** 035702 (2002).
[14] Y. Kafri, E. Levine, D. Mukamel and J. Török, *J. Phys. A: Math. Gen.* **35** L459 (2002).
[15] I. T. Georgiev, B. Schmittmann and R. K. P. Zia, *Phys. Rev. Lett.* **94** 115701 (2005).
[16] J. T. Mettetal, B. Schmittmann and R. K. P. Zia, *Europhys. Lett.* **58** 653 (2002).
[17] B. Schmittmann, J. T. Mettetal and R. K. P. Zia, in *Computer Simulation Studies in Condensed Matter Physics XVI*, eds. D.P. Landau, S.P. Lewis, and H. B. Schüttler (Springer, in press).
[18] G. Korniss, B. Schmittmann and R. K. P. Zia, unpublished (1999).
[19] M. E. J. Newman and G. T. Barkema, *Monte Carlo Methods in Statistical Physics.* Oxford University Press, Inc. (1999).
[20] P.C. Hohenberg and B.I. Halperin, Rev. Mod. Phys. 49, 435 (1977).
[21] G. Korniss, B. Schmittmann and R. K. P. Zia, *Europhys. Lett.* **32** 49 (1995) and *J. Stat. Phys.* **86** 721 (1997)
[22] P. F. Arndt and V. Rittenberg, *J. Stat. Phys* **107** 989 (2002)
[23] For a review, see G.M. Schütz, Integrable stochastic many-body systems. In: *Phase Transitions and Critical Phenomena*, Vol. 19, ed. by C. Domb and J.L. Lebowitz (Academic Press, New York 2001).
[24] B. Schmittmann, J.T. Mettetal, and R.K.P. Zia, In: *Computer Simulation Studies in Condensed Matter Physics* XVI, Eds. D.P. Landau, S.P. Lewis, and H.B. Schüttler, pp. 7-22 (Springer, Heidelberg 2004).
[25] J.L. Lebowitz, E. Presutti, and H. Spohn, *J. Stat. Phys.* **51**, 841 (1988)
[26] J. M. Burgers, *The nonlinear diffusion equation*, D. Reidel Publishing, Dordrecht (1974).
[27] E.D. Andjel, *Ann. Prob.* **10**, 525 (1982); for a review see M.R. Evans, *Braz. J. Phys.* **30**, 42 (2000).
[28] S. Grosskinsky, G.M. Schütz, and H. Spohn, J. Stat. Phys. **113**, 389 (2003); see also C. Godrèche, J. Phys. A **36**, 6313 (2003).
[29] S. Grosskinsky and T. Hanney, Phys. Rev. E **72**, 016129 (2005).